

# Analytical and Numerical Prediction of Concentration Profiles in Microfluidic Gradient Generators

Rob Chambers

May 19, 2007

## 1 Introduction

A host of recent microfluidic devices have been developed to create known and temporally stable chemical gradients. In one common design, a cascade of diffusive mixers recombine in a wide, shallow channel to yield an approximately linear concentration gradient.[1] The resulting concentration gradient can be used to study cell cell processes such as chemotaxis, differentiation, and proliferation. The concentration profile in these devices is often assumed to remain linear and constant throughout the length of the chamber, even though diffusion does cause the profile to decay. To combat this, high flow rates can be used to minimize the residence time of the fluid. However, high flow rates are known to impact the direction of cell migration. Consequently, a simple model of diffusion processes would be helpful in device design and evaluation. Presented below is an analytical model which employs Taylor-Aris dispersion to simplify the problem to 2-D steady-state diffusion. This problem is then solved using a separation of variables approach. Finally, the model's predictions are compared with those of full 3-D numerical simulation.

## 2 Theory

### 2.1 Taylor-Aris Dispersion

The coupling of diffusion with flow that is nonuniform in the transverse direction leads to potentially complex three-dimensional concentration gradients. An area averaging approach, however, allows us to simplify the three-dimensional convective diffusion equations to a two-dimensional approximation. First, we note that laminar fluid flow in a wide, shallow rectangular channel can be approximated, far from the side walls, as plane Poiseuille flow with velocity given by:

$$u(z) = \langle U \rangle + u'(z) = U_o + \frac{3}{2}U_o \left( \frac{1}{3} - \left( \frac{2z}{h} \right)^2 \right) \quad (1)$$

where  $U_o$  is the bulk velocity and  $h$  is the channel height. Here,  $\hat{x}$  is the streamwise direction,  $\hat{y}$  is the spanwise direction, and  $\hat{z}$  is the transverse direction. The full convective diffusion equation, then, is:

$$\frac{\partial c}{\partial t} + \vec{u}\nabla c = D\nabla^2 c \quad (2)$$

where  $c$  is concentration and  $D$  is intrinsic diffusivity. Noting that in this parallel flow  $v$  and  $w$  are zero, and that  $\frac{\partial c}{\partial t} = 0$ , Eq. 2 simplifies to:

$$u(z)\frac{\partial c}{\partial t} = D\nabla^2 c \quad (3)$$

Following Eq. 1, we express the concentration as the sum of a depth-averaged component and a perturbation:

$$c(x, y, z) = \langle c \rangle (x, y) + c'(x, y, z) \quad (4)$$

where  $\langle \dots \rangle$  denotes depth-averaging:

$$\langle f \rangle = \frac{1}{h} \int_{-h/2}^{h/2} f dz \quad (5)$$

Expanding  $u$  and  $c$  in this manner,

$$\langle u \rangle \frac{\partial \langle c \rangle}{\partial x} + \langle u \rangle \frac{\partial c'}{\partial x} + u' \frac{\partial \langle c \rangle}{\partial x} + u' \frac{\partial c'}{\partial x} = D\nabla^2 \langle c \rangle + D\nabla^2 c' \quad (6)$$

By definition,  $\langle c' \rangle = \langle u' \rangle = 0$ , and by the no-flux boundary conditions at the top and bottom walls  $\left\langle \frac{\partial^2 c}{\partial x^2} \right\rangle = \frac{\partial c}{\partial x} \Big|_{h/2} - \frac{\partial c}{\partial x} \Big|_{-h/2} = 0$ , so Eq. 6 reduces to:

$$\langle u \rangle \frac{\partial \langle c \rangle}{\partial x} = D\nabla^2 \langle c \rangle - \left\langle u' \frac{\partial c'}{\partial x} \right\rangle \quad (7)$$

Subtracting Eq. 7 from Eq. 6:

$$u' \frac{\partial \langle c \rangle}{\partial x} + \langle u \rangle \frac{\partial c'}{\partial x} + u' \frac{\partial c'}{\partial x} = D\nabla^2 c' + \left\langle u' \frac{\partial c'}{\partial x} \right\rangle \quad (8)$$

To further isolate the cross-correlation term, we nondimensionalize using the scalings  $x \sim L$ ,  $z \sim h$ ,  $y \sim w$ ,  $\langle c \rangle \sim C_o$ ,  $c' \sim C'_o$ ,  $\langle u \rangle \sim U_o$ , and  $u' \sim U_o$ , so that the left hand side of Eq. 8 becomes:

$$\frac{C_o U_o}{L} \frac{\partial \langle c \rangle}{\partial x} + \frac{C'_o U_o}{L} \langle u \rangle \frac{\partial c'}{\partial x} + \frac{C'_o U_o}{L} u' \frac{\partial c'}{\partial x} \quad (9)$$

and the right hand side becomes:

$$DC'_o \left( \frac{1}{L^2} \frac{\partial^2 c'}{\partial x^2} + \frac{1}{w^2} \frac{\partial^2 c'}{\partial y^2} + \frac{1}{h^2} \frac{\partial^2 c'}{\partial z^2} \right) + \frac{C'_o U_o}{L} \left\langle u' \frac{\partial c'}{\partial x} \right\rangle \quad (10)$$

Since we have required the geometry to be long and thin, we note that  $h \ll w$  and  $w \ll L$ . Further, we assume that  $C'_o \ll C_o$ . Dropping higher order terms and returning to dimensional form, we arrive at:

$$u' \frac{\partial \langle c \rangle}{\partial x} = D \frac{\partial^2 c'}{\partial z^2} \quad (11)$$

Because  $\frac{\partial \langle c \rangle}{\partial x}$  is not a function of  $z$ , we can take the depth-average of the entire left hand side and, substituting our expression for  $u'$  from Eq. 1,

$$\left\langle u' \frac{\partial c'}{\partial x} \right\rangle = \frac{1}{h} \int_{-h/2}^{h/2} \frac{3}{2} U_o \left( \frac{1}{3} - \left( \frac{2z}{h} \right)^2 \right) \frac{U_o h^2}{2D} \frac{\partial^2 \langle c \rangle}{\partial x^2} \left( \frac{z^2}{2h^2} - \frac{z^4}{h^4} \right) dz \quad (12)$$

$$= -\frac{U_o^2 h^2}{210D} \frac{\partial^2 \langle c \rangle}{\partial x^2} \quad (13)$$

Finally, substituting into Eq. , we arrive at the convective diffusion equation governing  $\langle c \rangle$ :

$$\langle u \rangle \frac{\partial \langle c \rangle}{\partial x} = D \nabla^2 \langle c \rangle - \left\langle u' \frac{\partial c'}{\partial x} \right\rangle \quad (14)$$

$$\langle u \rangle \frac{\partial \langle c \rangle}{\partial x} = D \left( \frac{\partial^2 \langle c \rangle}{\partial y^2} + \frac{\partial^2 \langle c \rangle}{\partial z^2} \right) + \left( D + \frac{U_o^2 h^2}{210D} \right) \frac{\partial^2 \langle c \rangle}{\partial x^2} \quad (15)$$

Thus, if the smallness parameters above are satisfied, depth-averaged concentration of the three dimensional system behaves as that of a two-dimensional system with an anisotropic diffusivity of  $D$  in the  $\hat{y}$  direction and  $D_{\text{eff}}$  in the  $\hat{x}$  direction, where:

$$D_{\text{eff}} = D + \frac{U_o^2 h^2}{210D} \quad (16)$$

(Note: calculation using the channel half-height would result in a coefficient of 2/105 instead of 1/210.) It will be helpful to our subsequent discussion to define a diffusivity ratio  $\gamma$ :

$$\gamma = \frac{D_{\text{eff}}}{D} = 1 + \frac{U_o^2 h^2}{210D^2} \quad (17)$$

Thus, for slow flows in shallow channels,  $\gamma$  can approach its minimum value of 1. However, there is no maximum  $\gamma$  as long as we remain in the Taylor-Aris regime, and the Taylor-Aris regime can always be obtained if the region of interest is sufficiently far downstream.

## 2.2 Transverse Concentration Gradients

In the previous section, a two-dimensional convective diffusion equation was derived to determine the depth-averaged concentration profile of a three-dimensional flow. Under conditions where this model is valid, knowledge of the fluid's velocity profile also enables the three-dimensional profile to be predicted from the results of the two-dimensional model. To begin, we rearrange Eq.11:

$$\frac{\partial^2 c'}{\partial z^2} = \frac{u'(z)}{D} \frac{\partial \langle c \rangle}{\partial x} \quad (18)$$

Since  $u'$  is known from Eq. 1, and if  $\frac{\partial \langle c \rangle}{\partial x}$  has been found by solution of the 2-D model, the right hand side of this equation is known. Consequently, we integrate Eq. 18:

$$\frac{\partial c'}{\partial z} = \frac{1}{D} \frac{\partial \langle c \rangle}{\partial x} \int \frac{3}{2} U_o \left( \frac{1}{3} - \left( \frac{2z}{h} \right)^2 \right) dz \quad (19)$$

$$= \frac{U_o z}{D h^2} \frac{\partial \langle c \rangle}{\partial x} \left( \frac{h^2}{4} - z^2 \right) + C_1(x, y) \quad (20)$$

By symmetry,  $\frac{\partial c'}{\partial z}|_{z=0} = 0$  for all  $(x, y)$ , so  $C_1 = 0$ . Integrating Eq. 20 again,

$$c' = \frac{U_o z^2}{D h^2} \frac{\partial \langle c \rangle}{\partial x} \left( \frac{h^2}{4} - \frac{z^2}{2} \right) + C_2(x, y) \quad (21)$$

Finally, by setting  $\langle c' \rangle = 0$  and adding the depth-averaged concentration  $\langle c \rangle$ , we arrive at an expression for the concentration at any point  $(x, y, z)$ , provided that the approximations of the Taylor Dispersion analysis hold:

$$c(x, y, z) = -\frac{U_o h^2}{480 D} \frac{\partial \langle c \rangle}{\partial x}(x, y) \left( 7 - 120 \left( \frac{z}{h} \right)^2 + 240 \left( \frac{z}{h} \right)^4 \right) \quad (22)$$

### 2.3 Solution of the 2-D Convective Diffusion Equation

Consider a long, thin channel of width  $2w$ , height  $h \ll 2w$ , and bulk-averaged fluid velocity  $U_o$ . Ignoring the attenuated flow near the channel edges, and applying the results of the Taylor-Aris dispersion analysis, we can model the system as uniform plug flow with velocity  $U_o$ , diffusivity  $D_{\text{eff}}$  in the streamwise direction  $\hat{x}$ , and diffusivity  $D$  in the spanwise direction  $\hat{y}$ . Under these assumptions, the concentration  $c$  of a dilute solute is governed by the 2-D convective diffusion equation:

$$U_o \frac{\partial c}{\partial x} = D_{\text{eff}} \frac{\partial^2 c}{\partial x^2} + D \frac{\partial^2 c}{\partial y^2} \quad (23)$$

Defining the nondimensional variables  $\xi = x/(w\sqrt{\gamma})$ ,  $\eta = y/w$ , and  $\Theta = (c - c_{\text{avg}})/c_o$ , the convective diffusion equation becomes:

$$\frac{U_o w}{\gamma D} \frac{\partial \Theta}{\partial \xi} = \frac{\partial^2 \Theta}{\partial \xi^2} + \frac{\partial^2 \Theta}{\partial \eta^2} \quad (24)$$

$$\text{Pe}_{\gamma, w} \frac{\partial \Theta}{\partial \xi} = \nabla^2 \Theta \quad (25)$$

where  $\gamma = D_{\text{eff}}/D$  (as in Eq. 17) and  $\text{Pe}_{\gamma, w} = U_o w / D \sqrt{\gamma}$ . Note that because  $\xi$  has been scaled by  $w\sqrt{\gamma}$ , the right hand side of Eq. 25 has become a Laplacian. The geometry and

inlet concentration profile then impose the boundary conditions:

$$\Theta(\xi = 0, \eta) = f(\eta) \quad (26)$$

$$\Theta_\xi(\xi = \infty, \eta) = 0 \quad (27)$$

$$\Theta_\eta(\xi, \eta = \pm 1) = 0 \quad (28)$$

Separating  $\Theta(\xi, \eta) = F(\xi)G(\eta)$ :

$$\frac{G''}{G} = \frac{-F'' + \text{Pe}_{\gamma,w}F'}{F} = -\lambda^2 \quad (29)$$

Using the boundary conditions of Eq. 28,  $\lambda = n\pi/2$  and  $G$  becomes a Fourier series:

$$G_n = a_n \sin \frac{n\pi}{2} \eta + b_n \cos \left( \frac{n\pi}{2} \right), n = 0, 1, 2, \dots \quad (30)$$

with the restriction that  $a_n=0$  for  $n$  even, and  $b_n=0$  for  $n$  odd. This sine-cosine series is attenuated for increasing  $\xi$  by the decaying exponential:

$$F_n = \exp \left\{ -\frac{\text{Pe}_{\gamma,w}}{2} \left( \sqrt{1 + \left( \frac{n\pi}{\text{Pe}_{\gamma,w}} \right)^2} - 1 \right) \xi \right\} \quad (31)$$

For small wavenumbers and large  $\text{Pe}_{\gamma,w}$ , this equation reduces to that obtained if Taylor Dispersion is neglected (i.e.,  $D_{\text{eff}} = D$  so that  $\gamma = 1$ ):

$$F_n = \exp \left\{ -\frac{(n\pi)^2}{2\text{Pe}_{\gamma,w}} \xi \right\} \quad (32)$$

For high wave numbers and small  $\text{Pe}_{\gamma,w}$ , the actual value of  $\text{Pe}_{\gamma,w}$  becomes irrelevant:

$$F_n = \exp \left\{ -\frac{n\pi}{2} \xi \right\} \quad (33)$$

Thus, the behavior of the concentration profile at low  $\xi$  is dominated by the attenuation of high-spatial-frequency components by spanwise diffusion. At large  $\xi$  these components vanish and the attenuating spanwise diffusion is partially counteracted by streamwise diffusion, which serves to maintain the profile further downstream.

In many practical applications, the region of interest is sufficiently far downstream that low-wave-number components are dominant. It is instructive to consider when, if ever, streamwise dispersion (as measured by  $\text{Pe}_{\gamma,w}$ ) significantly affects this region. By setting the second term inside the radical in Eq. 31 equal to one, and by considering the lowest wavenumber ( $n = 1$ ), we can estimate the crossover point  $\text{Pe}_c$  above which  $\text{Pe}_{\gamma,w}$  begins to dominate the system's far-field behavior:

$$\text{Pe}_{\gamma,w} = \text{Pe}_c \approx \pi \quad (34)$$

## 2.4 Fourier Series Approximation of Practical Concentration Profiles

The Fourier series formulation detailed above can represent any practical inlet concentration profile, and recent work has demonstrated nonlinear and even arbitrary profiles.[2] However, three inlet concentration profiles are of particular relevance to recent microfluidic gradient generators. With the concentration nondimensionalized as above, with  $\Theta = (c - c_{\text{avg}})/c_o$ , all three of these profiles are odd functions with no DC offset (i.e.,  $\Theta(\eta) = \Theta(-\eta)$ ), so that  $b_n = 0$  and the Fourier series reduces to a Fourier sine series.

The first profile of interest is a single *step profile* in which two initially uniform streams flow in parallel. This profile is represented by the Fourier coefficients:

$$a_n = \frac{4}{n\pi} \quad n = 1, 3, 5, \dots \quad (35)$$

The second profile of interest is the *staircase profile* which consists of  $k$  concentration steps. The step profile given above is simply a staircase profile with  $k = 2$ . For  $k$  odd, the Fourier coefficients of the staircase profile are given by:

$$a_n = \frac{8}{k-1} \sum_{j=1}^{\frac{k-1}{2}} \frac{\sin(n\pi j/k) \sin(n\pi/2)}{n\pi} \quad n = 1, 3, 5, \dots \quad (36)$$

The third profile of interest is the *linear profile*, which is an idealized staircase profile in which  $k \rightarrow \infty$ . While no inlet profile is truly linear, this idealization is often used with some success to predict downstream concentration gradients for devices with high  $k$ . Furthermore, the decay of its low-frequency components can be used to predict the far-field decay time of all three of these initial profiles. Its coefficients are given by:

$$a_n = \frac{8(-1)^{(n-1)/2}}{n^2\pi^2} \quad n = 1, 3, 5, \dots \quad (37)$$

While a Green's Function solution of the 2-D convective diffusion equation is possible, the Fourier Series formulation is simple for most common inlet concentration profiles. Further, the degree of development of a concentration profile can be estimated by comparing the magnitude of low-wavenumber components to the magnitude of high-wavenumber components, as in Fig. 1. For instance, in a simple *step profile*, the gradient might be considered sufficiently linear when the ratio of the magnitude of the  $n = 3$  wave to that of the  $n = 1$  wave reaches some critical value  $R_c$ . For this situation, combining Eqs. 35 and 31, we find the critical downstream position  $\xi_c$  to be:

$$\xi_c = -\frac{2 \ln(3R_c)}{\text{Pe}_{\gamma,w}} \left[ \left( \sqrt{1 + \left( \frac{3\pi}{\text{Pe}_{\gamma,w}} \right)^2} - \sqrt{1 + \left( \frac{\pi}{\text{Pe}_{\gamma,w}} \right)^2} \right) \right]^{-1} \quad (38)$$

Similar calculations can determine, for example, the number of steps needed in a *staircase profile* or the required  $\text{Pe}_{\gamma,w}$  in any profile to reach a given figure of merit.

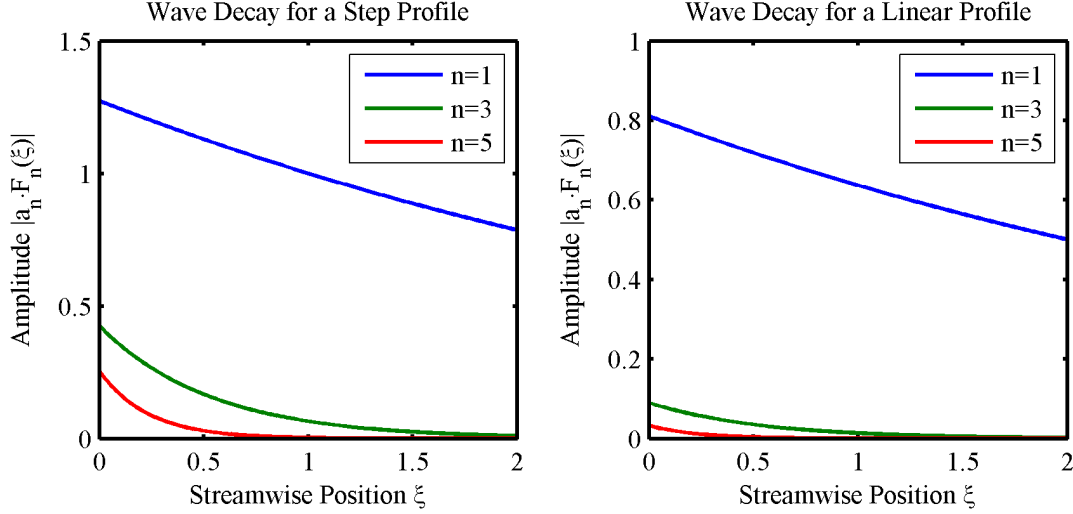


Figure 1: Decay of wave components of a step (left) and linear (right) inlet concentration profile. Plotted is wave amplitude  $|a_n \cdot F_n(\xi)|$  for  $\text{Pe}_{\gamma,w} = 10$ . The relative magnitude of the  $n = 1$  and  $n = 3$  waves can be used as a measure of how developed the profile is at a given  $\xi$ .

### 3 3-D Numerical Simulation

A model of the 3-D convective diffusion problem was implemented in COMSOL Multiphysics. The diffusion chamber was represented as a rectangular prism. Following the nondimensionalization used above, the chamber had a width in the  $\hat{y}$  direction of 2, a height in the  $\hat{z}$  direction of  $\alpha = h/w$ , and a length in the  $\hat{x}$  direction of  $L/w$ .

Diffusion was implemented with the convective diffusion function of COMSOL's MEMS Module. The isotropic diffusivity was arbitrarily set to  $D = 1$ . Fluid velocity was modeled as above, with

$$u(z) = \text{Pe}_w \frac{3}{2} \left( 1 - \left( \frac{2z}{\alpha} \right)^2 \right) \quad (39)$$

Consequently, the physics of the model were prescribed by entirely by the Peclet number  $\text{Pe}_w$  and the aspect ratio  $\alpha$ . Adaptive mesh refinement was used to bring the number of mesh elements to roughly 30,000.

## 4 Results

Simulation results for two cases are presented below. The first, *Case A*, uses the same parameters and an initial concentration profile as Lin et al.[1] The second, *Case B*, modifies those parameters slightly to bring the problem further into the Taylor Dispersion regime.

Note that Case A does *not* fulfill the condition that  $\frac{U_o h^2}{DL} \ll 1$ ; consequently, transverse concentration gradients may be significant.

	$2 \cdot w$ [ $\mu\text{m}$ ]	$U_o$ [ $\mu\text{m/s}$ ]	$h$ [ $\mu\text{m}$ ]	$L$ [cm]
Case A	175	380	100	1.2
Case B	400	100	50	1.2

Table 1: Dimensional Parameters

	$\text{Pe}_w$	$\gamma$	$\frac{U_o h^2}{DL}$	$\frac{\gamma}{.1 \cdot \text{Pe}_w^2}$
Case A	222	77	1.1	.016
Case B	133000	2.3	.070	$1.3 \cdot 10^{-9}$

Table 2: Nondimensional Parameters

Both cases used a 7-step staircase profile at the fluid inlet. Results results of the numerical simulation of case B are shown in Fig. 2, and more detailed analysis follows below.

## 4.1 Transverse Concentration Gradients

While the analytical model developed in previous sections predicts a 2-D depth-averaged concentration, most applications of microfluidic gradient generators require knowledge of the 3-D field. For instance, experiments involving adherent cells depend on concentrations near the chamber wall, which can differ from those along the centerline. Furthermore, even transverse gradients may affect cell behavior.

Plotted in Fig. 3 are concentration profiles in Case A at the chamber wall and at the centerline for  $\xi = .05$  and  $\xi = 1$ . These positions corresponding to downstream distances of  $8.75\mu\text{m}$  and  $175\mu\text{m}$ , and smallness parameters  $\frac{U_o h^2}{DL}$  of 1500 and 75, respectively. Encouragingly, the transverse variation essentially vanishes by  $\xi = 1$ , even though the smallness parameter is clearly much greater than 1. In the region of interest at  $L = 1.2\text{cm}$ , variations are virtually nonexistent.

## 4.2 Downstream Concentration Profiles

Figures 4 and 5 show predicted downstream concentration profiles for cases A and B. Due to the length of the chamber in these simulations, computer memory constraints limited the accuracy of the numerical solution for small  $\xi$  in case A. However, both cases show excellent agreement between analytical and numerical predictions.

## 5 Conclusion

Overall, the analytical model appears to accurately predict concentration profiles in practically relevant cases. It could prove useful both in performing rough calculations of concentration profiles during device design, and in optimizing device geometries and flow rates. Further development of the model could center around the effects of flow attenuation near the edges of the chamber, or on determining a smallness parameter which better describes



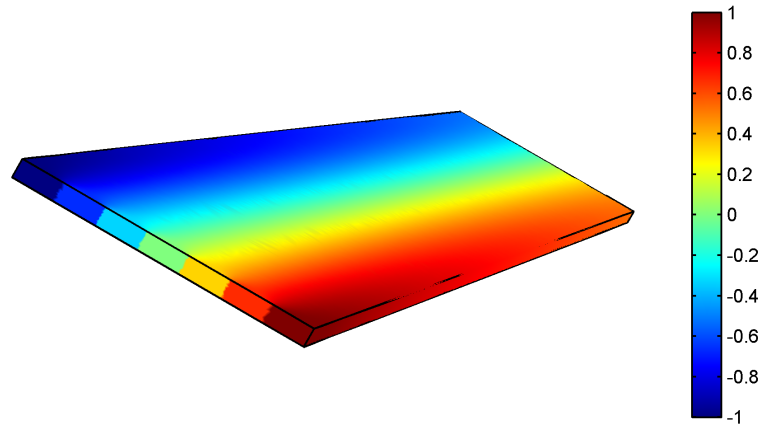


Figure 2: Boundary plot of a 3-D simulation of case B. The inlet concentration profile consists of seven "steps" of equal width. This profile is quickly smoothed by diffusion, and becomes a decaying half-cosine downstream. These profiles are shown more quantitatively in Fig. 5.

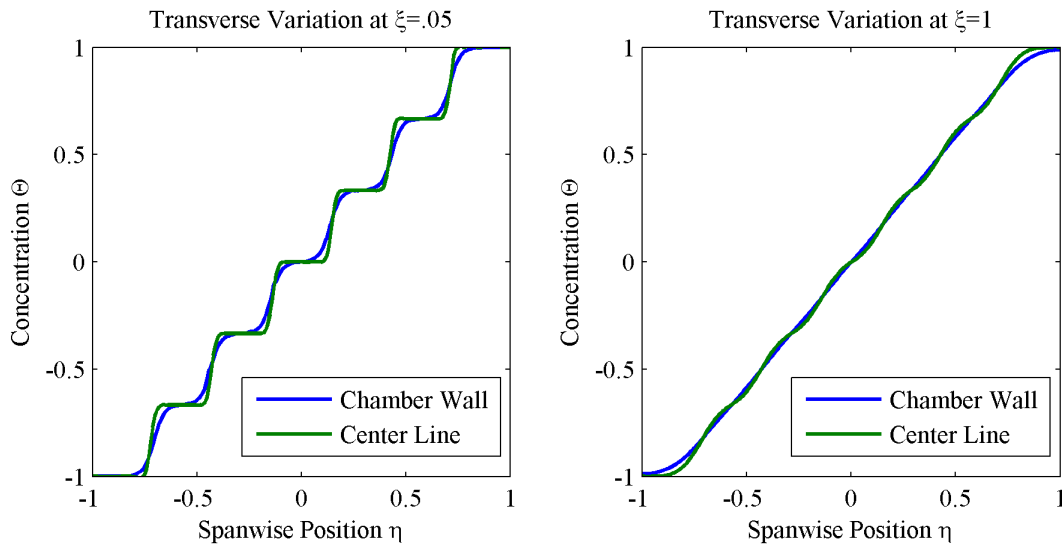


Figure 3: Concentration profiles for case A at  $\xi = .05$  and  $\xi = 1$ , for both the center of the chamber and the chamber wall. The significant differences between the two profiles close to the inlet (left) are substantially smoothed downstream (right).

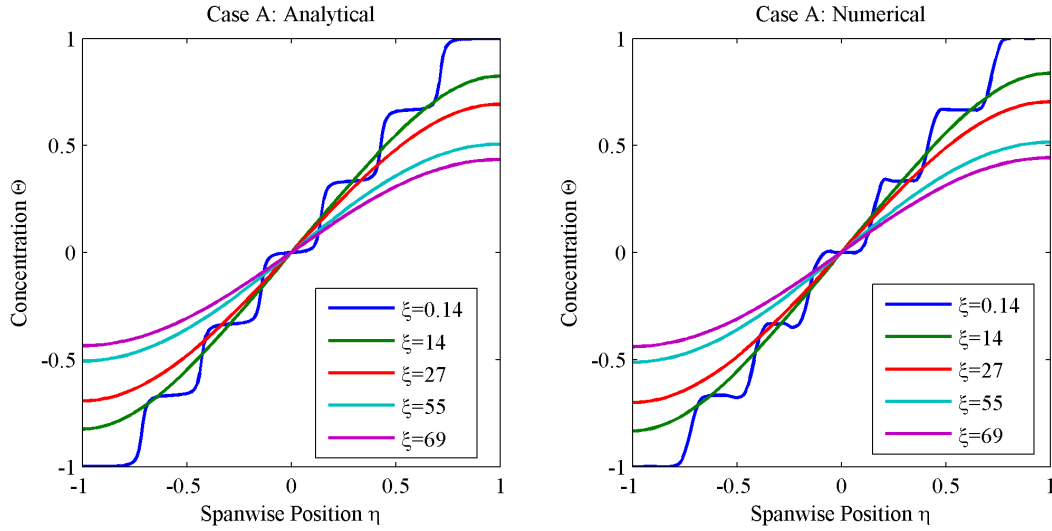


Figure 4: Concentration profiles for case A at several streamwise positions. The analytical and numerical predictions show excellent agreement. The numerical results for  $\xi = .14$  are impacted by the resolution of the mesh; however, more detailed results are shown in Fig. 2. Numerical measurements are taken at the centerline.

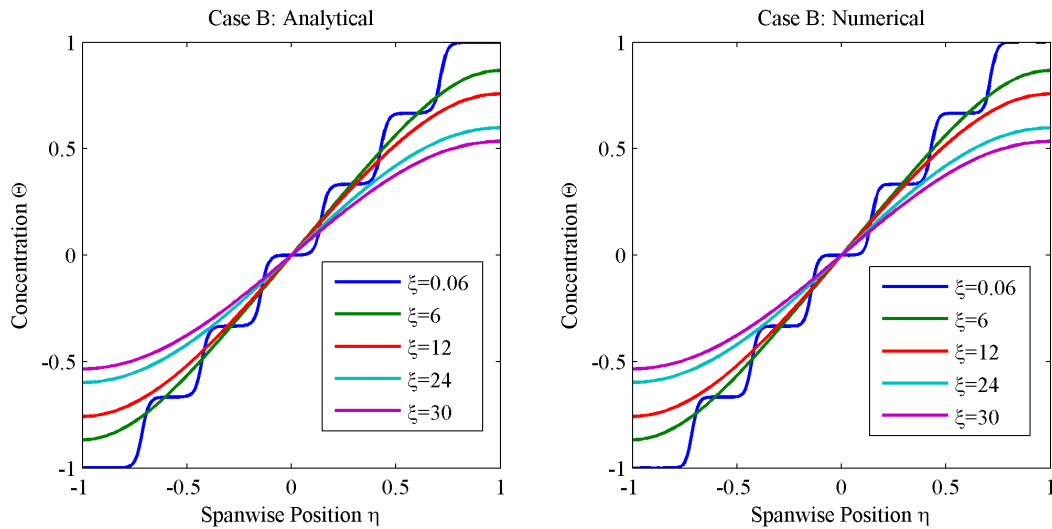


Figure 5: Concentration profiles for case B at several streamwise positions. As in case A, the analytical and numerical predictions show excellent agreement.

the regime in which the model is accurate. Finally, comparison with experimental data, as opposed to numerical predictions, could provide much more rigorous validation.

## References

- [1] F. Lin, C. M. C. Nguyen, S. J. Wang, W. Saadi, S. P. Gross, and N. L. Jeon, “Effective neutrophil chemotaxis is strongly influenced by mean il-8 concentration,” *Biochemical and Biophysical Research Communications*, vol. 319, no. 2, pp. 576–581, 2004.
- [2] D. Irimia, D. A. Geba, and M. Toner, “Universal microfluidic gradient generator,” *Analytical Chemistry*, vol. 78, no. 10, pp. 3472–3477, 2006.